Chinese Chemical Letters 37 (2026) 111844

Contents lists available at ScienceDirect

Chinese Chemical Letters

journal homepage: www.elsevier.com/locate/cclet

Aqueously dispersed homopolypeptide nanotoroids with tunable circularly polarized luminescence

Yuanpeng Ye[b,1], Xinke Hu[b,1], Dong Yang[b,1], Qianxi Gu[a], Shangning Liu[a], Jinhui Jiang[c,*], Guofeng Liu[d,*], Jianzhong Du[a,b,c,e,*]

[a] Department of Polymeric Materials, School of Materials Science and Engineering, Tongji University, Shanghai 201804, China
[b] Guohao College, Tongji University, Shanghai 200092, China
[c] Department of Gynaecology and Obstetrics, Shanghai Key Laboratory of Anesthesiology and Brain Functional Modulation, Clinical Research Center for Anesthesiology and Perioperative Medicine Translational Research Institute of Brain and Brain-Like Intelligence, Shanghai Fourth People's Hospital, School of Medicine, Tongji University, Shanghai 200434, China
[d] Shanghai Key Laboratory of Chemical Assessment and Sustainability, School of Chemical Science and Engineering, Advanced Research Institute, Tongji University, Shanghai 200092, China
[e] School of Materials Science and Engineering, East China University of Science and Technology, Shanghai 200237, China

ARTICLE INFO

Article history:
Received 10 June 2025
Revised 14 September 2025
Accepted 16 September 2025
Available online 16 September 2025

Keywords:
Circularly polarized luminescence
Homopolypeptide
Self-assembly
Nanotoroid
Reactive oxygen species

ABSTRACT

Aqueously dispersed nanomaterials exhibiting circularly polarized luminescence (CPL) hold great potentials in biological fields due to the inherent chirality of biological systems and its excellent biocompatibility. However, the limited availability of biodegradable CPL nanoparticles in aqueous media has severely constrained the development of biomedical CPL. Here, we present a facile strategy for achieving tunable CPL of aqueously dispersed nanotoroids through the co-assembly of a homopolypeptide with three achiral triphenylamine derivatives, showing a CPL performance depending on the architecture and doping content of small molecules. Remarkably, a deep-red CPL can be achieved with a record luminescence dissymmetry factor ($g_{lum} = 1.1 \times 10^{-2}$) among aqueously polypeptide-based nanoparticles. Furthermore, the densely packed nanostructure completely suppressed the intrinsic reactive oxygen species generation of the chromophores by restricting oxygen diffusion and quenching exciton-energy transfer, thereby eliminating phototoxic risks while preserving imaging fidelity. Overall, this work not only provides a facile method for achieving aqueous CPL from achiral molecules but also establishes a structure-property relationship between chromophore geometry and supramolecular CPL performance, advancing their potential in biological fields.

© 2026 Published by Elsevier B.V. on behalf of Chinese Chemical Society and Institute of Materia Medica, Chinese Academy of Medical Sciences.

Circularly polarized luminescence (CPL), characterized by the emission of chiral photons with defined handedness, represents a unique photophysical phenomenon that encodes stereochemical information into light. Distinct from conventional unpolarized luminescence, CPL provides an additional dimension of chirality, enabling its utility in fields such as optoelectronics, information encryption, asymmetric synthesis, and biomedicine [1–4]. Among these applications, biomedical CPL nanomaterials have gained growing attention in recent years [5–7]. Such interest stems from the intrinsic chirality of biological systems, a ubiquitous feature exemplified by biomacromolecules (*e.g.*, DNA, proteins, polysaccharides) and cellular architectures [8–10]. This inherent dissymmetry between CPL and biological chirality has motivated investigations into chirality-mediated bioeffects like cell differentiation [11]. In addition, CPL-enhanced contrast agents exhibit unique capability to suppress biological autofluorescence through chiral discrimination mechanisms, enabling background-free imaging with subcellular-level resolution [12,13]. Overall, biomedical CPL nanomaterials hold transformative potential for decoding chiral signals in pathological processes and advancing therapeutic development [14,15]. However, there are two critical challenges in this field: (1) The scarcity of aqueously dispersed CPL nanoparticles compatible with physiological environments, and (2) the predominance of non-biodegradable, heavy metal-containing architectures in existing aqueous CPL platforms, which raise unresolved concerns regarding systemic biocompatibility and long-term biosafety [14,16–19]. Therefore, it is crucial to develop aqueous CPL nanomaterials with good biodegradability.

* Corresponding authors.
E-mail addresses: Jinhui_JIANG@alumni.tongji.edu.cn (J. Jiang), liuguofeng@tongji.edu.cn (G. Liu), jzdu@tongji.edu.cn (J. Du).
[1] These authors contributed equally to this work.

https://doi.org/10.1016/j.cclet.2025.111844
1001-8417/© 2026 Published by Elsevier B.V. on behalf of Chinese Chemical Society and Institute of Materia Medica, Chinese Academy of Medical Sciences.

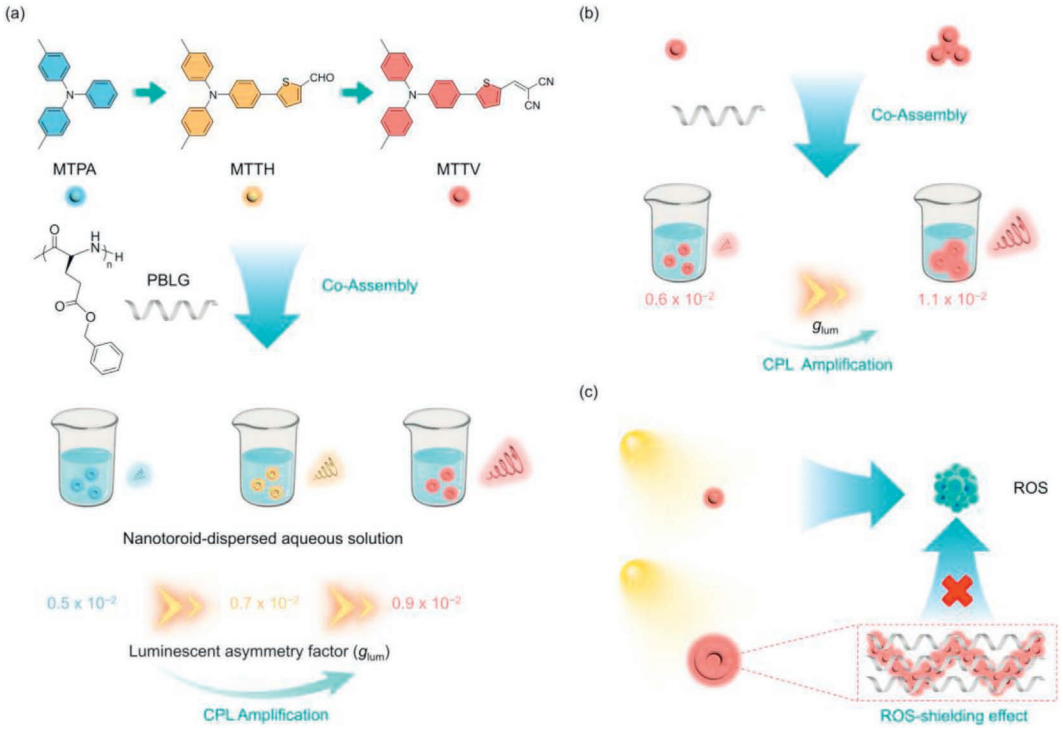


Fig. 1. Aqueously dispersed nanotoroids exhibiting tunable circularly polarized luminescence (CPL) and suppressed reactive oxygen species (ROS) activity. (a) Chemical structure-dominated CPL through co-assembly of poly(γ-benzyl-L-glutamate) (PBLG) with achiral triphenylamine derivatives of 4-methyl-*N*-phenyl-*N*-(*p*-tolyl)aniline (MTPA), 5-(4-(di-*p*-tolylamino)phenyl)thiophene-2-carbaldehyde (MTTH), and 2-((5-(4-(di-*p*-tolylamino)phenyl)thiophen-2-yl)methylene)malononitrile (MTTV). (b) Dose-dependent CPL in the co-assembly of PBLG@MTTV. (c) ROS-shielding effect in the co-assembly of PBLG@MTTV.

Polypeptides exhibit structural homology to natural proteins [20–23]. This biomimetic architecture endows them with exceptional biocompatibility and biodegradability [24–26]. Crucially, polypeptides can form higher-order nanostructures with chirally organized polymer chains due to their inherent molecular chirality and regular secondary structures originated from chiral amino acids, facilitating the formation of chiroptically active nanomaterials. In 2023, Jiang *et al*. demonstrated an aqueous CPL nanoparticle *via* the self-assembly of poly(γ-benzyl glutamate) terminated with an achiral fluorescent chromophore [27]. While this approach achieved stable CPL emission in the aqueous media, it relied on a pre-synthesized fluorescent initiator to covalently terminate the polypeptide chains, necessitating a multi-step synthesis protocol that limits scalability and modularity. Although the study highlighted the potential of co-assembly with the achiral small molecule to amplify chiroptical activity, only monochromatic CPL was achieved with relatively low luminescence dissymmetry factor ($g_{lum} < 10^{-2}$). Moreover, it remains unclear about the structure influence of doped small molecules on the emergent chiroptical properties. Consequently, it is unknown about the universality of this strategy by replacing the achiral dye and whether tunable aqueous CPL with amplified properties can be achieved.

Herein, aqueously dispersed nanotoroids were successfully prepared *via* the co-assembly of poly(γ-benzyl-L-glutamate) (PBLG) with three achiral triphenylamine derivatives (Fig. 1a). These solutions exhibited multicolor chiral emissions with tunable CPL performance regulated by the architecture of achiral molecules as well as their doping content in the co-assembly. Our results demonstrate that superior CPL properties can be obtained by co-assembly with achiral molecules of twisted intramolecular charge-transfer (TICT) characteristics, which can be attributed the enhanced compatibility between the twisted molecular conformations of the triphenylamine derivatives and the helically ordered phenyl groups of PBLG. Furthermore, a positive correlation can be found between the CPL property and doping content in co-assembly, enabling the deep-red CPL with a maximum g_{lum} up to 10^{-2} (Fig. 1b). Additionally, the reactive oxygen species (ROS) activity of these TICT-active triphenylamine derivatives can be completely suppressed following co-assembly (Fig. 1c), suggesting potential applications for long-term *in vivo* imaging with minimized biological injury in the future.

A donor-acceptor (D-A) configured triphenylamine derivative usually functioned as an achiral chromophore for CPL amplification when co-assembled with chiral poly(γ-benzyl glutamate) [28]. However, the mechanistic necessity of the D-A architecture for both CPL generation and amplification in such co-assembly remains ambiguous. To address this fundamental structure-property correlation, three triphenylamine derivatives: 4-methyl-*N*-phenyl-*N*-(*p*-tolyl)aniline (MTPA), 5-(4-(di-*p*-tolylamino)phenyl)thiophene-2-carbaldehyde (MTTH), and 2-((5-(4-(di-*p*-tolylamino)phenyl)thiophen-2-yl)methylene)malononitrile (MTTV), were strategically designed as molecular probes to interrogate the role of electronic and steric configurations in chiroptical induction *via* PBLG-mediated co-assembly (Fig. 2a). Comprehensive synthetic procedures and structural characterization data for MTTH, MTTV, and PBLG are provided in Supporting information (Scheme S1 and Figs. S1-S5 in Supporting information).

The photophysical behaviors of MTPA, MTTH, and MTTV were systematically compared. In tetrahydrofuran (THF), all three derivatives exhibited a locally excited (LE) absorption band centered at ~300 nm, characteristic of $\pi \rightarrow \pi^*$ transitions in their aromatic frameworks (Fig. 2b). Notably, MTTH and MTTV displayed additional redshifted absorption bands at 410 and 500 nm, respectively, attributed to intramolecular charge-transfer (ICT) transitions arising from their D-A architectures. The corresponding fluorescence spectra under ultraviolet (UV) excitation revealed distinct emission maxima at 370 nm (near-UV), 530 nm (yellow), and

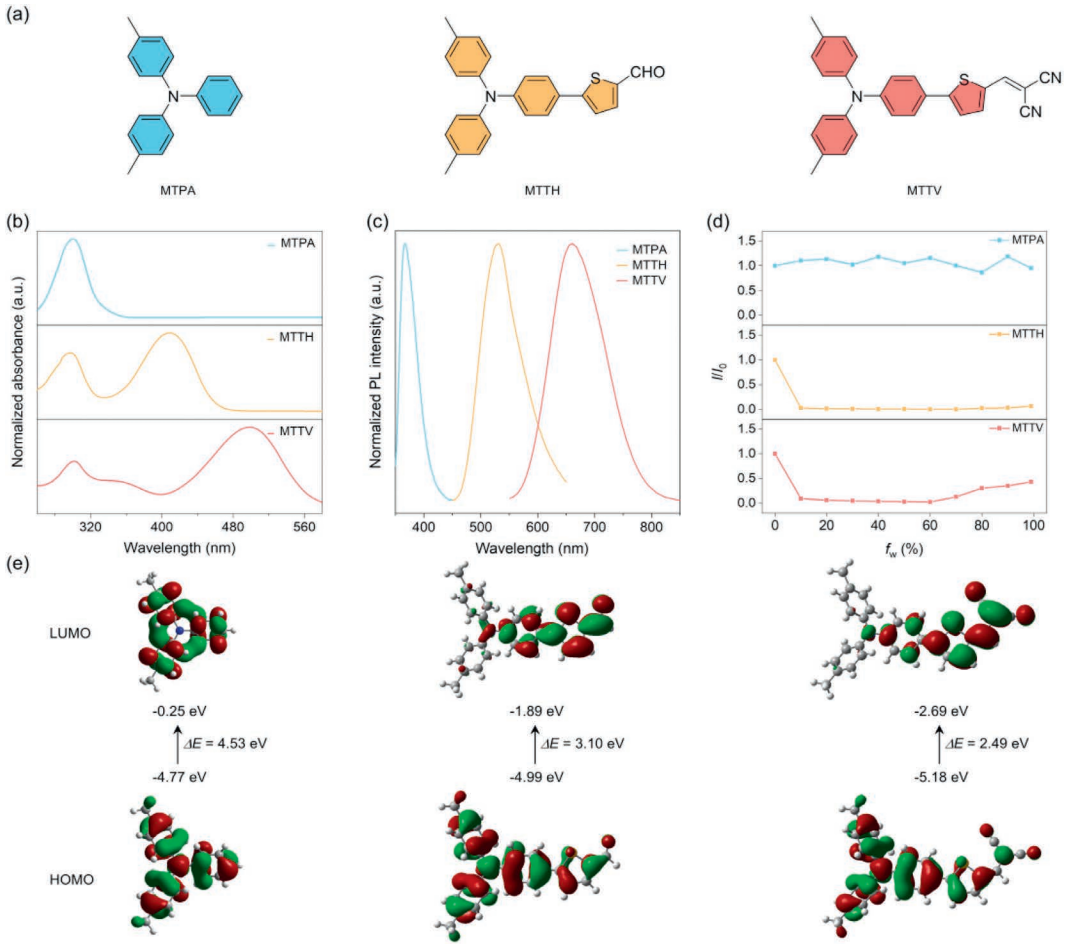


Fig. 2. Photophysical properties of three triphenylamine derivatives dissolved in tetrahydrofuran (THF). (a) Chemical structures of MTPA, MTTH, and MTTV. (b) Normalized absorption spectra. Concentration (c) = 10 μmol/L. (c) Normalized photoluminescence (PL) spectra. c = 10 μmol/L, λ_{ex} (MTPA) = 300 nm, λ_{ex} (MTTH) = λ_{ex} (MTTV) = 365 nm. (d) Plots of relative PL intensity (I/I_0) *versus* f_w. c = 10 μmol/L, λ_{ex} (MTPA) = 300 nm, λ_{ex} (MTTH) = λ_{ex} (MTTV) = 365 nm, f_w is defined as the water fraction in THF/water mixtures, I_0 = PL intensity at f_w = 0%. (e) Density functional theory (DFT) calculation (B3LYP/6–31G(d), Gaussian 16) results of MTPA, MTTH, and MTTV: energy diagram, HOMO, and LUMO.

660 nm (deep-red) for MTPA, MTTH, and MTTV, respectively (Fig. 2c), with emission colors reflecting progressive ICT enhancement across the series. When water was added into the THF solution as a poor solvent, different photoluminescence (PL) behaviors were exhibited from these three derivatives (Fig. 2d and Fig. S6 in Supporting information). While MTPA maintained stable PL intensity across f_w (referred to the volume fraction of water in the THF/water mixture) from 0 to 99%, MTTH and MTTV exhibited pronounced PL quenching. Specifically, their PL intensities sharply declined at f_w = 10%, followed by progressive attenuation until f_w = 60%, and marginal recovery at higher f_w. This behavior aligns with TICT mechanisms, wherein polar environments stabilize non-radiative decay pathways [29,30]. Density functional theory (DFT) calculations elucidated the frontier molecular orbital distributions (Fig. 2e). For MTPA, HOMO density localized on the electron-rich triphenylamine core, while LUMO occupied π^* orbitals of benzene rings, reflecting minimal ICT due to its symmetric structure. Introducing a thiophene-carbaldehyde unit strengthened D-A interactions in MTTH, concentrating HOMO on the triphenylamine donor and delocalizing LUMO toward the carbaldehyde acceptor. Through the further incorporation of the strong electron-withdrawing malononitrile group, a pronounced charge separation was presented in MTTV with HOMO partially delocalized into the thiophene bridge and LUMO highly localized on the malononitrile acceptor. Therefore, the progressive enhancement of ICT from MTPA to MTTV contributed to red-shifted absorption/emission bands and the water-responsive PL behaviors.

Subsequently, the three co-assembly systems were respectively performed in THF by the solvent-switching method. Specifically, incremental additions of water were introduced into pre-mixed solutions of PBLG ([PBLG] = 1.0 mg/mL) and each small molecule ([MTPA] = [MTTH] = [MTTV] = 0.2 mmol/L). Dynamic light scattering (DLS) analysis confirmed the formation of well-defined nanostructures across all assemblies. The apparent hydrodynamic diameters ($D_{h,app}$s) were 358, 363, and 364 nm with all narrow polydispersities (PDs < 0.1) for nanoparticles composed of PBLG@MTPA, PBLG@MTTH, and PBLG@MTTV, respectively (Fig. 3a). Morphological characterization by transmission electron microscopy (TEM) and scanning electron microscopy (SEM) further revealed toroidal nanostructures with diameters of approximately 400 nm (Fig. 3b). These results indicate the molecular structure of the incorporated small molecules exerts negligible influence on the aggregation mode of PBLG during co-assembly.

The corresponding photophysical properties were investigated for these nanotoroid aqueous dispersion. Emission maxima were observed at 370 nm (PBLG@MTPA), 525 nm (PBLG@MTTH), and 648 nm (PBLG@MTTV), respectively (Fig. 3c). Notably, MTTH and MTTV exhibited blue-shifted emissions in the toroidal state compared to their dissolved counterparts in THF, which can be attributed to the restricted TICT in the aggregated state. To confirm

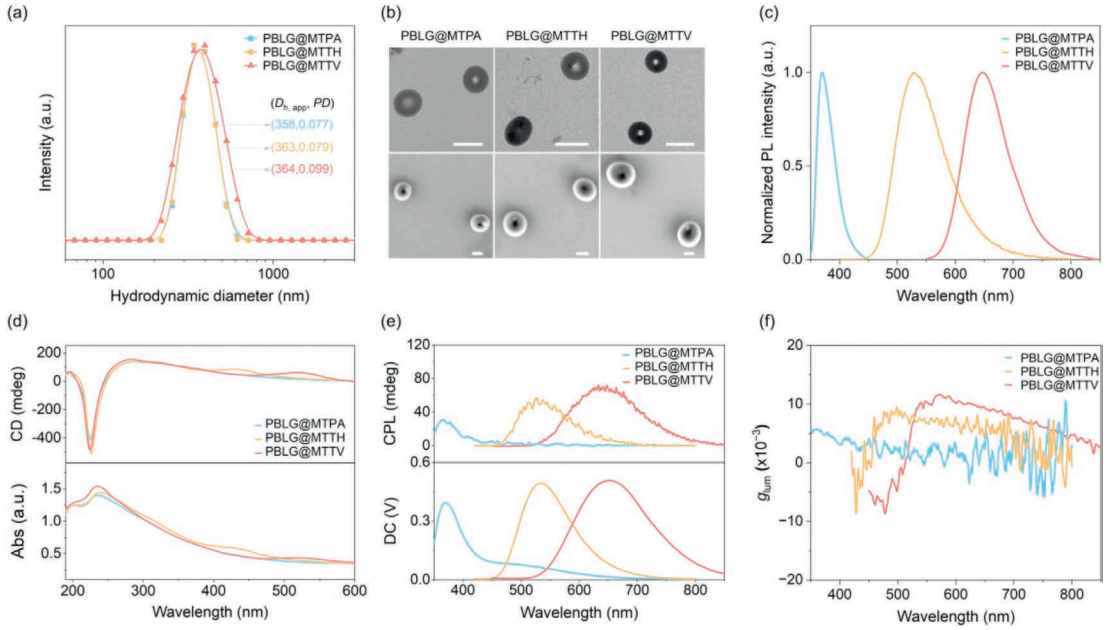


Fig. 3. Nanostructures and photophysical properties of aqueously dispersed nanotoroids obtained in co-assembly architectures of PBLG@MTPA, PBLG@MTTH, and PBLG@MTTV. (a) Dynamic light scattering (DLS) results. $c = 0.20$ mg/mL. (b) Transmission electron microscopy (TEM) and scanning electron microscopy (SEM) images. Scale bar: 200 nm. (c) Normalized PL spectra. $c = 0.20$ mg/mL, λ_{ex} (MTPA) = 300 nm, λ_{ex} (MTTH) = λ_{ex} (MTTV) = 365 nm. (d) Circular dichroism (CD) spectra. $c = 0.04$ mg/mL. (e) CPL spectra. $c = 0.20$ mg/mL, λ_{ex} (MTPA) = 300 nm, λ_{ex} (MTTH) = λ_{ex} (MTTV) = 365 nm. (f) Luminescence dissymmetry factor (g_{lum}) curves. $c = 0.20$ mg/mL, λ_{ex} (MTPA) = 300 nm, λ_{ex} (MTTH) = λ_{ex} (MTTV) = 365 nm. The initial concentration for PBLG and each small molecule in THF was kept as 1.0 mg/mL and 0.2 mmol/L, respectively.

chiral transfer from the helical PBLG matrix to the achiral triphenylamine derivatives during co-assembly, circular dichroism (CD) and CPL analyses were conducted. As shown in Fig. 3d, CD spectra displayed characteristic negative bands at 210–240 nm for all assemblies, corresponding to the n→π^* transitions of PBLG's α-helical peptide bonds. Additionally, a positive CD signal at 260 nm emerged for each assembly, attributed to the chiral packing of PBLG's pendant phenyl groups *via* π–π stacking, which spectrally overlapped with LE absorption bands of MTPA, MTTH, and MTTV. Meanwhile, distinct CD signals were clearly presented and aligned with ICT absorption bands of MTTH and MTTV (Fig. S7 in Supporting information), indicating a D-A structure induced chiral amplification. Furthermore, all nanotoroid-dispersed solutions displayed positive CPL signals matched with the near UV, yellow, and red emissions with the corresponding luminescence dissymmetry factors (g_{lum}s) of 0.5×10^{-2}, 0.7×10^{-2}, and 0.9×10^{-2} for PBLG@MTPA, PBLG@MTTH, and PBLG@MTTV, respectively (Figs. 3e and f). These results highlight the critical role of D-A architectures in amplifying chiroptical activity, likely due to enhanced compatibility between the twisted molecular conformations of the triphenylamine derivatives and the helically ordered phenyl groups of PBLG.

The content of an achiral D-A guest significantly influences the CPL property in a similar co-assembly process [31]. To investigate the tunability of CPL in the PBLG@MTTV co-assembly, varying amounts of MTTV (0.1, 0.2, and 0.4 mmol/L) were used to form nanoparticles through the same assembly process. Similar toroidal nanostructures were confirmed by DLS, TEM, and SEM measurements (Figs. 4a and b), suggesting that the co-assembly process was minimally affected by the amount of MTTV. Notably, a red-shifted emission from 630 nm to 660 nm was observed as the doping concentration increased from 0.1 mmol/L to 0.4 mmol/L (Fig. 4c). CD measurements revealed similar Cotton effects across the samples, accompanied by red-shifted CD peaks matching the ICT absorption band of MTTV in the 500–600 nm range (Fig. 4d). Meanwhile, the CPL property of PBLG@MTTV solution displayed a positive correlation with the MTTV content, with the g_{lum} value increasing from 0.6×10^{-2} to 1.1×10^{-2} (Figs. 4e and f). These results demonstrate that higher doping ratios of MTTV promote stronger π–π stacking interactions among the MTTV molecules, resulting in a red-shifted fluorescence. When more achiral MTTV molecules participate in co-assembly, they are more effectively transferred into a chirally packed state by the chiral space formed from helically packed PBLG chains [27], leading to the amplified CPL.

Triphenylamine derivatives featuring D-A architectures have been extensively engineered for bioimaging applications owing to their notable photostability and high fluorescence quantum yields [32]. However, such compounds often exhibit intrinsic reactivity for generating ROS, posing risks of cellular or tissue damage during prolonged imaging protocols. To address this critical limitation, we systematically evaluated the ROS generation capacity of the PBLG@MTTV co-assembly in aqueous media using 2,7-dichlorofluorescin diacetate (DCFH) as a fluorogenic probe, which undergoes oxidation to fluorescent 2,7-dichlorofluorescein (DCF) upon ROS interaction. As shown in Fig. 5a, the control experiments with DCFH alone exhibited negligible fluorescence under white light irradiation (4 mW/cm^2, 5 min). In stark contrast, free MTTV triggered a 47-fold increase in DCF fluorescence intensity under identical conditions, confirming its potent ROS generation capability (Fig. 5b). Strikingly, the PBLG@MTTV exhibited negligible fluorescence enhancement, demonstrating effective ROS suppression (Figs. 5c and d). Meanwhile, a similar ROS-shielding effect can be still observed for PBLG@MTTH despite the inherently weaker ROS activity for the free MTTH (Fig. S8 in Supporting information). Compared with other normally soft polymer matrixes for encapsulating similar photosensitizers to achieve nice ROS performance [33,34], this novel ROS-shielding effect may be attributed to the tight packing of PBLG chains that can hinder the permeation of oxygen and water, reducing ROS generation and diffusion. This unique co-assembly structure not only preserves the chiroptical fidelity required for CPL bioimaging but also mitigates phototoxicity, thereby enabling the potential application for long-term *in vivo* imaging with minimized biological injury.

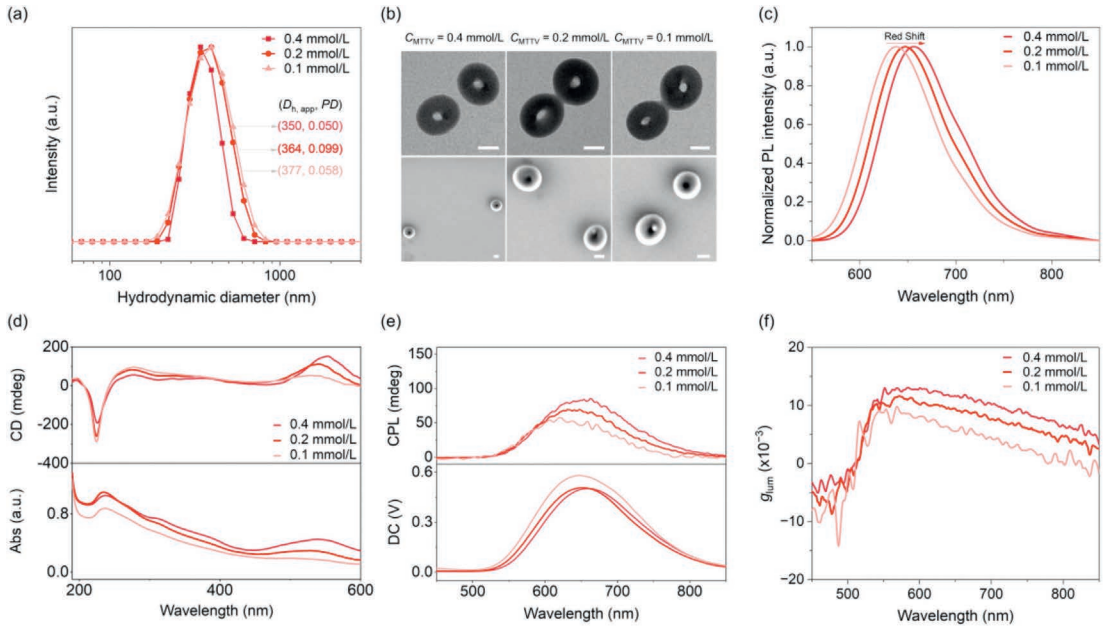


Fig. 4. Nanostructures and photophysical properties of aqueously dispersed nanotoroids obtained with different initial concentrations of MTTV (C_{MTTV}s) in the co-assembly architectures of PBLG@MTTV. (a) DLS results. $c = 0.20$ mg/mL. (b) TEM and SEM images. Scale bar: 200 nm. (c) Normalized PL spectra. $c = 0.20$ mg/mL, $\lambda_{ex} = 365$ nm. (d) CD spectra. $c = 0.04$ mg/mL. (e) CPL spectra. $c = 0.20$ mg/mL, $\lambda_{ex} = 365$ nm. (f) g_{lum} curves. $c = 0.20$ mg/mL, $\lambda_{ex} = 365$ nm. "$C_{MTTV} = 0.4$ mmol/L" refers to the initial concentration of MTTV dissolved in THF was 0.4 mmol/L, where the initial concentration of PBLG was fixed at 1.0 mg/mL.

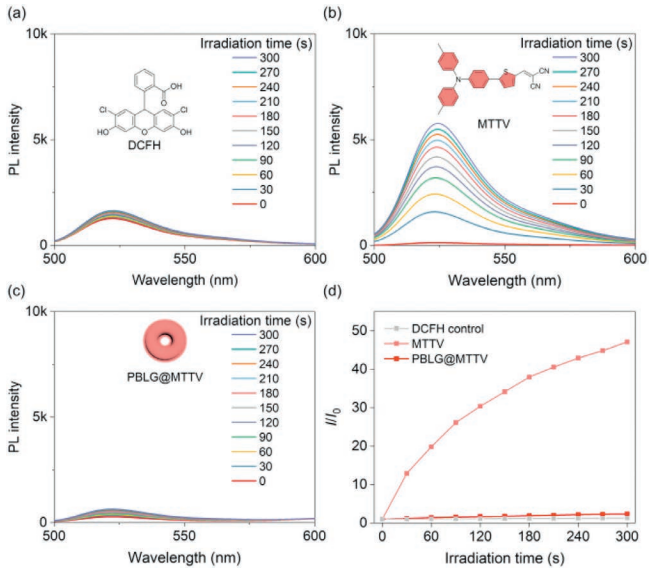


Fig. 5. Chemical trapping of total ROS generation. (a) Photoactivation of 2,7-dichlorofluorescin diacetate (DCFH). (b) Photoactivation of DCFH with MTTV. (c) Photoactivation of DCFH with PBLG@MTTV. (d) Activation rates of DCFH under different conditions at 525 nm emission. All measurements were carried out under white light irradiation (4 mW/cm^2, 5 min) in 1× PBS buffer. All PL spectra were obtained upon the excitation of 488 nm. [MTTV] = [MTTV]$_{PBLG@MTTV}$ = 10 μmol/L.

In summary, we developed a facile strategy for achieving tunable CPL in aqueous media by the co-assembly of PBLG with achiral triphenylamine derivatives (MTPA, MTTH, and MTTV). This approach enabled the preparation of aqueously dispersed nanotoroids exhibiting multicolor CPL emissions: spanning near-UV, yellow, and deep-red regimes, with progressively enhanced CPL performance. Mechanistically, the TICT characteristics of the triphenylamine derivatives facilitated stereochemical compatibility between their nonplanar conformations and the helically ordered phenyl motifs of PBLG, thereby optimizing chirality transfer efficiency and amplifying g_{lum}. Crucially, modulating the doping content of MTTV within the co-assembly nanoparticle allowed precise control over both emission wavelength and chiroptical intensity, culminating in deep-red CPL at 660 nm with a record g_{lum} of 1.1×10^{-2} for aqueously polypeptide-based CPL nanoparticles. Furthermore, the densely packed PBLG matrix suppressed ROS generation by sterically hindering the permeation of oxygen and water, thereby eliminating phototoxic risks while preserving imaging fidelity. This work not only provides a facile method for achieving aqueous CPL through the co-assembly of homopolypeptides with achiral small molecules but also reveals the structure-property relationship in the chiral phenomenon, which can promote the development of polypeptide-based CPL nanomaterials for potential biomedical applications.

Declaration of competing interest

The authors declare that they have no known competing financial interests or personal relationships that could have appeared to influence the work reported in this paper.

CRediT authorship contribution statement

Yuanpeng Ye: Writing – original draft, Formal analysis, Conceptualization. **Xinke Hu:** Formal analysis. **Dong Yang:** Formal analysis. **Qianxi Gu:** Formal analysis. **Shangning Liu:** Formal analysis. **Jinhui Jiang:** Writing – original draft, Project administration, Formal analysis, Conceptualization. **Guofeng Liu:** Project administration, Funding acquisition. **Jianzhong Du:** Project administration, Funding acquisition.

Acknowledgments

This research is supported by the National Natural Science Foundation of China (Nos. 22471198, 22101208, 22335005), and Innovation Program of Shanghai Municipal Education Commission (No. 2023ZKZD28), and the Fundamental Research Funds for the Central Universities.

Supplementary materials

Supplementary material associated with this article can be found, in the online version, at doi:10.1016/j.cclet.2025.111844.

References

[1] J. Kumar, T. Nakashima, T. Kawai, J. Phys. Chem. Lett. 6 (2015) 3445–3452.
[2] G. Longhi, E. Castiglioni, J. Koshoubu, et al., Chirality 28 (2016) 696–707.
[3] J. Roose, B.Z. Tang, K.S. Wong, Small 12 (2016) 6495–6512.
[4] Y. Zhang, S. Yu, B. Han, et al., Matter 5 (2022) 837–875.
[5] Q. Miao, X. Wang, B.W. Jin, et al., J. Mater. Chem. C 12 (2024) 4861–4869.
[6] Z.T. Shi, Q. Wang, J.H. Yi, et al., Angew. Chem. Int. Ed. 61 (2022) e202207405.
[7] Y.P. Liu, P.Y. Xing, Adv. Mater. 35 (2023) 2300968.
[8] Q. Gao, L.L. Tan, Z.H. Wen, et al., Nano Res. 16 (2023) 11107–11124.
[9] V.A. Tverdislov, E.V. Malyshko, Phys. Usp. 62 (2019) 354–363.
[10] L.T. Guo, Y.Q. Guo, R. Wang, et al., Molecules 28 (2023) 5629.
[11] P. Stachelek, L. MacKenzie, D. Parker, R. Pal, Nat. Commun. 13 (2022) 553.
[12] H. Koike, K. Nozaki, M. Iwamura, Chem. Asian J. 15 (2020) 85–90.
[13] P. Stachelek, S. Serrano-Buitrago, B.L. Maroto, et al., ACS Appl. Mater. Interfaces 16 (2024) 67246–67254.
[14] Y.K. Dai, J.Q. Chen, C.Q. Zhao, et al., Angew. Chem. Int. Ed. 61 (2022) e202211822.
[15] Y.T. Sang, J.L. Han, T.H. Zhao, et al., Adv. Mater. 32 (2020) 1900110.
[16] G.Y. Wang, H.Y. Zhang, H. Kuang, et al., Matter 6 (2023) 1752–1781.
[17] N.H. Cho, H. Kim, J.W. Kim, et al., Chem 10 (2024) 1052–1070.
[18] C. Zhang, S. Li, X.Y. Dong, S.Q. Zang, Aggregate 2 (2021) e48.
[19] C.L. Hao, G.Y. Wang, C. Chen, et al., Nano-Micro Lett. 15 (2023) 39.
[20] Z.Y. Song, Z.Y. Han, S.X. Lv, et al., Chem. Soc. Rev. 46 (2017) 6570–6599.
[21] A.R. Mazo, S. Allison-Logan, F. Karimi, et al., Chem. Soc. Rev. 49 (2020) 4737–4834.
[22] Z.Y. Song, H.L. Fu, R. Wang, et al., Chem. Soc. Rev. 47 (2018) 7401–7425.
[23] T. Li, X.M. Lu, M.R. Zhang, et al., Bioact. Mater. 11 (2022) 268–282.
[24] M. Stepanova, A. Nikiforov, T. Tennikova, E. Korzhikova-Vlakh, Pharmaceutics 15 (2023) 2641.
[25] L. Tan, R. Huan, L.F. Wu, et al., Mini-Rev. Med. Chem. 23 (2023) 399–411.
[26] S. Zhang, T. Chen, J. Lin, et al., Polym. Bull. 17 (2004) 19–28.
[27] J.H. Jiang, F.L. Ma, R.H. Dong, et al., J. Am. Chem. Soc. 145 (2023) 27282–27294.
[28] Y.C. Guo, Y.F. Zhang, J.F. Ma, et al., Nat. Commun. 15 (2024) 9303.
[29] S. Sasaki, G.P.C. Drummen, G. Konishi, J. Mater. Chem. C 4 (2016) 2731–2743.
[30] K. Hanaoka, S. Iwaki, K. Yagi, et al., J. Am. Chem. Soc. 144 (2022) 19778–19790.
[31] F. Wang, C.S. Shen, F.W. Gan, et al., CCS Chem. 5 (2023) 1592–1601.
[32] Z.Q. Xu, Y.B. Luo, X.M. Yang, et al., J. Photochem. Photobiol. A 444 (2023) 115002.
[33] W.B. Wu, D. Mao, S.D. Xu, et al., Chem 4 (2018) 1937–1951.
[34] J.C. Ni, Y.J. Wang, H.K. Zhang, et al., Molecules 26 (2021) 268.